Maritime Technology and Research

https://so04.tci-thaijo.org/index.php/MTR

Research Article

Tether analysis and stability investigation of space rocket launch offshore compliant platform in regular seas

Srinivasan Chandrasekaran[1,2,*], Ashish Unnikrishnan[1] and Adwait Panindre[1]

[1]*Department of Ocean Engineering, Indian Institute of Technology Madras, Chennai, India*
[2]*Faculty of International Maritime Studies, Kasetsart University, Sriracha campus, Chonburi 20230, Thailand*

[*]*Corresponding author's e-mail address: drsekaran@iitm.ac.in*

Article information
Received: October 8, 2024
Revision: January 17, 2025
Accepted: January 26, 2025

Keywords
Floating structure;
Triceratops;
Mathieu stability;
Offshore structure;
Stability analysis

Abstract
This study investigates the stability of a multi-utility offshore platform designed for rocket launches, focusing on tether dynamics and platform behavior under operational and failure scenarios. The platform, modeled in ANSYS AQWA, features buoyant legs and a topside connected by ball-and-socket joints, allowing translational motion while maintaining independent rotations. The extended topside introduces pitch moments requiring stability checks. Free-decay tests reveal rigid heave and pitch motions (~3 s) and flexible surge motions (~150 s). Dynamic tether analysis under various sea states highlights that simultaneous tether failures critically affect platform stability, causing significant shifts in heave and pitch.

1. Introduction

Recent studies focused on harnessing marine environments for sustainable and eco-friendly space launches. Traditional marine rocket launching methods have relied on fixed platforms and monolithic floating platforms (Zhengyu et al., 2021). Fixed platforms are limited to shallower waters, restricting access to deep-sea locations and optimal launch sites. Additionally, their proximity to land complicates the process of obtaining environmental clearance. Deep-water floating platforms, such as drillships and semi-submersibles, address this limitation. However, these platforms are considered monolithic structures, where the hull and topside are rigidly connected, meaning that wave-induced moments on the hull are directly transferred to the topside, potentially destabilizing the platform. Moreover, the forces from rocket launches are transmitted to the hull, necessitating an expensive hull design. To overcome these issues with deep-water monolithic floating platforms, Chandrasekaran (2017) and Ashish et al. (2024) emphasized the benefits of offshore topside-legs isolated platforms, offshore Triceratops, compared to traditional marine launch methods. These are positively buoyant platforms anchored to the seabed with high-tension tethers. Since these platforms are operating within dynamic equilibrium, they are more prone to instability triggered by eccentric impacts on the topside. Additionally, due to tether tensioning, assessing stability is crucial to ensure operational safety (Suja & Chandrasekaran, 2025; Chandrasekaran & Chinu, 2023). Hence, stability analysis becomes pivotal in determining stability under impact forces. This study analyzes tether responses under various failure scenarios to capture the instabilities caused by tether dislodgement during launches. Although the stability of positively buoyant structures has been explored in earlier studies, the analysis of platform stability during tether removal, particularly under the influence of high rocket thrust impacts, represents a novel contribution. This study extends previous research by considering the unique dynamic challenges posed by tether dislodgement in the context of rocket launches, where significant thrust forces are applied to the platform.

The Mathieu stability parameters are widely recommended for the hydrodynamic stability analysis of floating structures (Koo et al., 2004; Allievi & Soudack, 1990), with numerical charts available from Kolukula (2012). The stability being considered in this study is not the structural stability typically assessed through buckling analysis, but rather the hydrodynamic stability of the offshore platform, which is commonly analyzed using Mathieu's equation. While Mathieu's stability relies on hydrodynamic parameters, structural stability is influenced by a structure's geometry. Mathieu stability assumes free-body conditions and is independent of material properties, whereas structural stability involves specific boundary conditions and is dependent on the material properties of the structure. Mathieu's equation requires the variation in tether tension as its input, which must be derived from the hydrodynamic analysis of the structure.

Some research work on cable breakage in offshore structures is described below as background to the work presented in this paper. Patel and Park (1991) explored the behavior of TLP tethers when subjected to low pre-tension, focusing on the effects of wave-induced time-varying axial forces. Their study highlighted that reduced pre-tension, while advantageous for increasing payload, introduces parametric oscillations governed by the nonlinear Mathieu equation. The research derived the governing partial differential equation for tether lateral motion and reduced it to a simplified nonlinear Mathieu equation using Galerkin's method and separation of variables. By developing Mathieu stability charts over a broad range of parameters, the study addressed the oscillatory behavior in the first instability region, and extended the analysis to higher instability regions using numerical methods, including the fourth-order Runge-Kutta approach.

Recently, Chandrasekaran and Kiran (2018) investigated the stability of the offshore Triceratops platform through numerical modeling and dynamic analyses to assess the impact of wave loads on tether stability using Mathieu stability principles. The results demonstrated that increased payload induces tether instability, with platform instability occurring prior to tether failure in the analyzed cases. This research highlights the critical interplay between payload variations and the dynamic stability of compliant offshore platforms.

Furthermore, Haitao et al. (2023) examined the dynamic behavior of a tension leg platform (TLP) under various damaged mooring conditions using a nonlinear hull-tendon model developed in ANSYS AQWA. The model incorporates the coupling effects between platform motion and mooring line dynamics at each time step. A novel method for simulating tendon breakage was proposed, enabling the study of transient effects, platform responses to both simultaneous and progressive tendon failures, and the platform's performance changes post-failure. The findings reveal that tendon breakage significantly impacts the dynamic responses and overall platform performance. The study emphasizes the importance of assessing tendon breakage scenarios in advance to ensure platform safety and mitigate potential risks.

Hence, this study employs numerical analysis using ANSYS AQWA to understand the platform's hydrodynamic characteristics and develop stability parameters for assessing tether stability during rocket launch, using stability charts. The study explores hypothetical scenarios of tether removal, hence the name postulated, which may not directly represent real-world conditions. However, tether removal could occur during accidental events such as collisions, ice loads, or fatigue due to variable submergence. Additionally, snap loads from initial elongation could lead to plastic deformation. Analyzing tether failure is crucial for understanding the survivability of the structure in these situations.

2. Numerical analysis

2.1 Offshore Triceratops rigid body dynamics

The force equilibrium of a 3-legged rocket launching Triceratops (**Figure 1**) in the vertical plane is given by Ashish et al. (2024) as:

$$F_B = W + 3(T_T) + F_T \tag{1}$$

Where F_B is the buoyancy force, W is the sum of the weight of the platform and the payload, T_T is the initial pretension in the tethers, and F_T is the thrust force from the rocket launch. The thrust force, F_T, is calculated using the relation:

$$F_T = \dot{m}v_e + (P_e - P_a)A_e \tag{2}$$

Where $\dot{m}$ is the mass flow rate of the propellant, v_e is the exhaust velocity, P_e is the exit pressure, P_a is the ambient pressure, and A_e is the nozzle exit area. This formulation is derived from the conservation of momentum and energy for rocket propulsion (Mishra, 2017). Furthermore, it is important to note that Triceratops is designed for a high degree of positive buoyancy. The equation of motion is given as:

$$[M + M_a]\{\ddot{x}\} + [C]\{\dot{x}\} + [K]\{x\} = \{F(t)\} \tag{3}$$

Where *[M]* is the mass matrix, *[M$_a$]* is the added mass matrix, *[C]* is the damping matrix, and *[K]* is the stiffness matrix of the offshore Triceratops. Further, $\{\ddot{x}\}, \{\dot{x}\}, and\ \{x\}$ are the platform's acceleration, velocity, and displacement vectors in all the degrees of freedom, while $\{F(t)\}$ is the external exciting force. The platform's mass is the sum of the mass of the deck, buoyant legs, payload, and the rocket load. The added mass due to variable submergence, caused by large displacements in flexible degrees of freedom, is accounted for separately. Chandrasekaran et al. (2013) discussed the derivation of mass, stiffness, damping, and hydrodynamic coefficients from the rudimentary stage. The exciting force is a sum of the hydrodynamic and the rocket launch force, $F_w(t)$ and $R(t)$respectively, acting on the platform. The corresponding matrices are given as follows:

$$\{F(t)\} = \{F_w(t)\} + \{R(t)\} \tag{4}$$

As the constituents of the equation of motion are response-dependent, which is a typical case in offshore compliant structures, it is solved by the average acceleration method (Newmark, 1959).

2.2 Hydrodynamic and stability analysis

The hydrodynamic performance of the offshore platform was analyzed using ANSYS AQWA, considering wave-induced forces, platform dynamics, and tether interactions under operational and failure scenarios. The analysis employed linear wave theory, assuming the fluid to be incompressible, inviscid, and governed by irrotational flow. These assumptions are valid for deep-water conditions where wave steepness remains small. The wave height and period were selected based on Indian Ocean conditions, with significant wave heights ranging from 2 m to 10 m and peak wave periods from 6 s to 15 s (Anusree & Sanil Kumar, 2023; Sabique et al., 2012). For the numerical simulations, average values within these ranges were used to represent regular sea states, ensuring a computationally efficient approach. Hence, in this study, regular sea conditions (wave height of 6 m and a period of 10 s) were used to evaluate the hydrodynamic response of the offshore structure. Regular waves were chosen to simplify the analysis and focus on fundamental system dynamics under tether failure conditions. This approach provides a basis for understanding the structure's response to postulated tether failures, which can be extended to more complex wave spectra in future studies.

The offshore platform under consideration comprises of buoyant legs connected to the topside by ball joints (**Figure 1**), allowing the transfer of translational but restraining rotation between them. Supported by three buoyant legs, the Triceratops features a triangular topside. Ashish et al. (2024) outline detailed structural characteristics and analysis methods, including mathematical formulations solved using the average acceleration method.

Design parameters shown in **Table 1** guide the structural and geometric inputs for numerical analysis. The topside is modeled as a rigid structure with mass concentrated at the center of mass. Modeled as surface elements, the platform's topside is connected to buoyant legs through ball joints. The ball and socket joint mechanism (**Figure 2**) plays a crucial role in limiting excessive motion of the offshore platform, particularly during dynamic loading conditions. By allowing independent rotational motion while sharing translational movement between the topside and the buoyant legs, the ball joints reduce the transmission of forces that could lead to excessive motion or instability. The ball-and-socket joint mechanism plays a pivotal role in preventing instability transfer to the deck by allowing rotational freedom. Although AQWA does not explicitly capture this mechanism, its effect on overall system stability was considered in the selection of boundary conditions and constraints.

A rocket, with a thrust force of approximately 1,000 kN and a base time of 0.8 s, is launched from the extended topside (**Figure 3**). High-tensioned tethers connect the Triceratops to the seabed, which is crucial for stability during production and launch due to its high buoyancy. Each leg carries four such tethers: tethers 1 - 4 to leg 1, tethers 5 - 8 to leg 2, and tethers 9 - 12 to leg 3. Tether failure was simulated by incrementally removing tension elements in the numerical model. This allowed the assessment of stability under progressive failure scenarios, with particular attention to shifts in heave and pitch mean positions. Simultaneous tether failure was identified as the most critical, leading to significant instability in the platform.

The stability of the offshore platform was evaluated by analyzing its dynamic behavior under operational and failure scenarios using the Mathieu stability equation. The tether tension derived from the hydrodynamic analysis served as the primary input for assessing stability. Under regular sea conditions (wave height of 6 m and a period of 10 s), the standard form of the Mathieu equation is given in (1) and (2) as follows:

$$\frac{d^2x}{dt^2} + (\delta + q\cos(t))x = 0 \tag{5}$$

Where δ and q are Mathieu parameters, while x is a variable depending on the independent variable t. These parameters are derived according to Patel and Park (1991) and given below:

$$\delta = \frac{(2\varpi)^2}{\omega^2};\ q = \frac{2S\varpi^2}{P\omega^2};\ \varpi = \frac{\pi}{L}\sqrt{\frac{P}{M}} \tag{6}$$

Where ϖ is the frequency of the first mode of free vibration of a loaded tether (in rad/s), L is the length of the tether (in m), M is the mass per unit length of the tether (in kg/m), and ω is the wave frequency (in rad/s). P and S are the average tether tension (in N) and amplitude of tether tension variation (in N), respectively. The tether tension derived from the hydrodynamic analysis of the structure serves as input to the Mathieu stability equation, which is then used to determine the stability parameters. Under tether failure scenarios, the effective stiffness reduces significantly, altering the δ parameter and potentially pushing the system into unstable regions of the Mathieu stability diagram.

Table 1 Structural details of Triceratops with rocket launcher (Ashish et al., 2024).

Description	Details		
Material	steel		
Water depth (h)	2,400 m		
Length of topside	95 m		
Depth of topside	12 m		
Area of topside	3,933 m^2		
Shape of leg	circular		
Diameter of leg (D_{BL})	15 m		
c/c distance between legs (P_b)	61.77 m		
Length of the buoyant leg (L_{BL})	174.24 m		
Freeboard	20.24 m		
Draft (d)	154 m		
Meta-centric height	51.38 m		
Unit weight of steel	7,850 kg/m^3		
Topside weight + payload	187.56 MN		
Weight of legs	75 MN		
Ballast weight	309 MN		
Buoyancy per leg	280. 75 MN		
Rotational parameters of topside			
Center of mass about x-axis	0 m		
Center of mass about y-axis	0 m		
Center of mass about z-axis	26.24 m		
Radius of gyration about x-axis	27.15 m		
Radius of gyration about y-axis	27.15 m		
Radius of gyration about z-axis	33.97 m		
Rotational parameters of legs			
	Leg 1	**Leg 2**	**Leg 3**
Center of mass about x-axis	39.778 m	-19.922 m	-19.922 m
Center of mass about y-axis	0	34.5 m	-34.5 m
Center of mass about z-axis	-110.34 m	-110.34 m	-110.34 m
Radius of gyration about x-axis	51.54 m	51.54 m	51.54 m
Radius of gyration about y-axis	51.54 m	51.54 m	51.54 m
Radius of gyration about z-axis	7.29 m	7.29 m	7.29 m

3. Results and discussion

3.1 Dynamic response verification

The dynamic response of the platform is assessed to determine natural frequencies for three degrees of freedom: surge, heave, and pitch. The natural period for surge (~150 s) indicates flexible behavior, while heave and pitch (~3 s) shows high rigidity due to tether constraints. The developed model is validated by comparing the computed natural periods of the platform’s degrees of freedom with results from previous studies (**Table 2**). The compliance of the offshore Triceratops structure, characterized by stiffness in some degrees of freedom (low natural period) and flexibility in others (high natural period), plays a critical role in its dynamic behavior. The agreement between the present and referenced models verifies that the present model accurately captures this essential characteristic. However, the observed difference in the natural period for surge compared to the reference study can be attributed to the inclusion of the extended rocket launch platform's additional mass and variations in the water depth considered in the analysis.

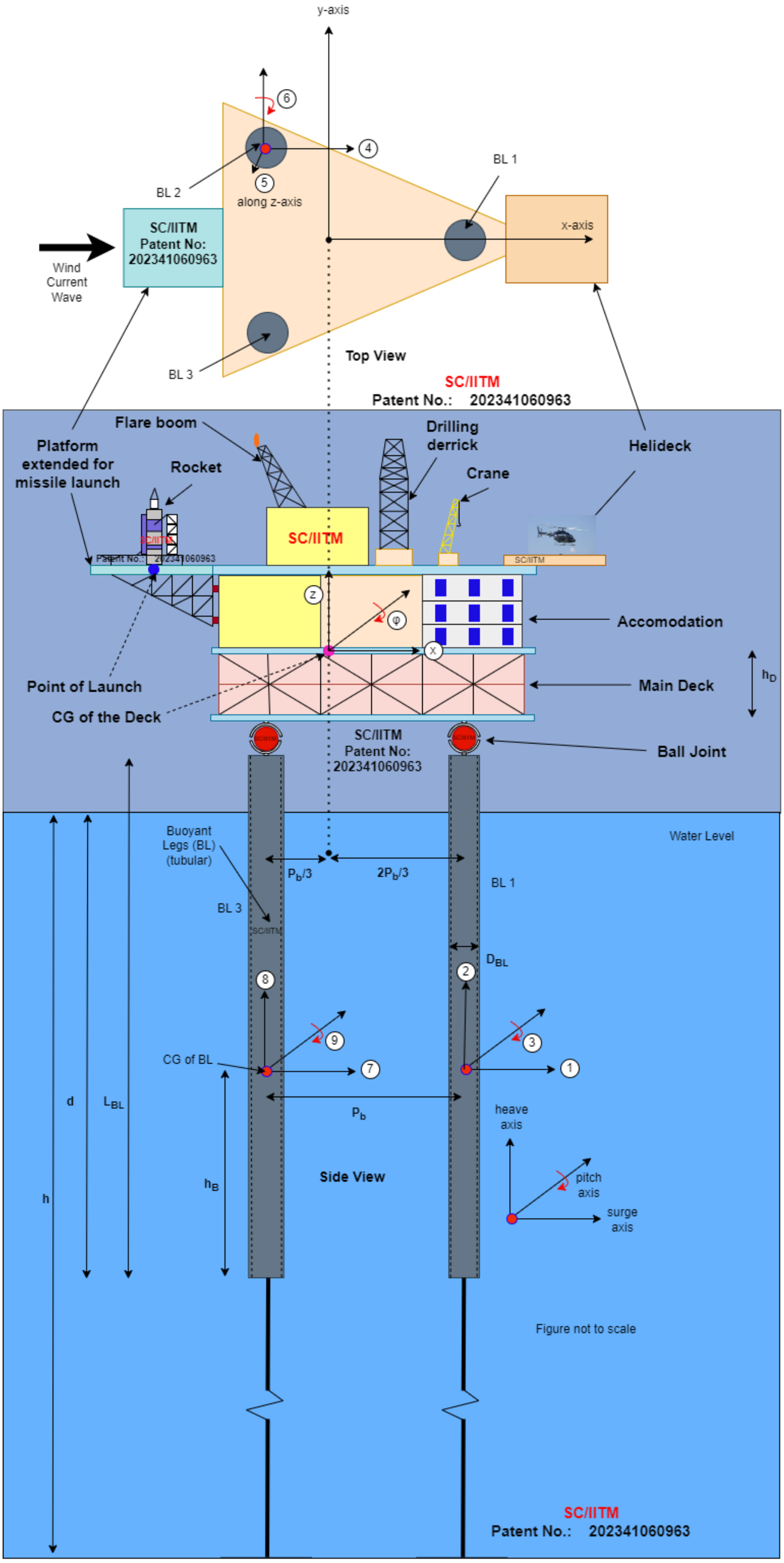

Figure 1 Conceptual model of rocket launching Triceratops^{patented} platform (Patent No.: 202341060963).

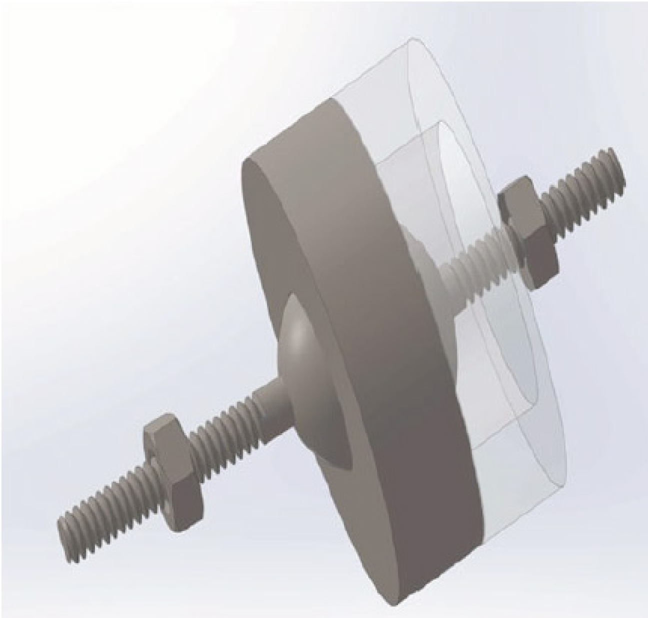

Figure 2 Conceptual model of ball and socket joint (Chandrasekaran & Mayanak, 2016).

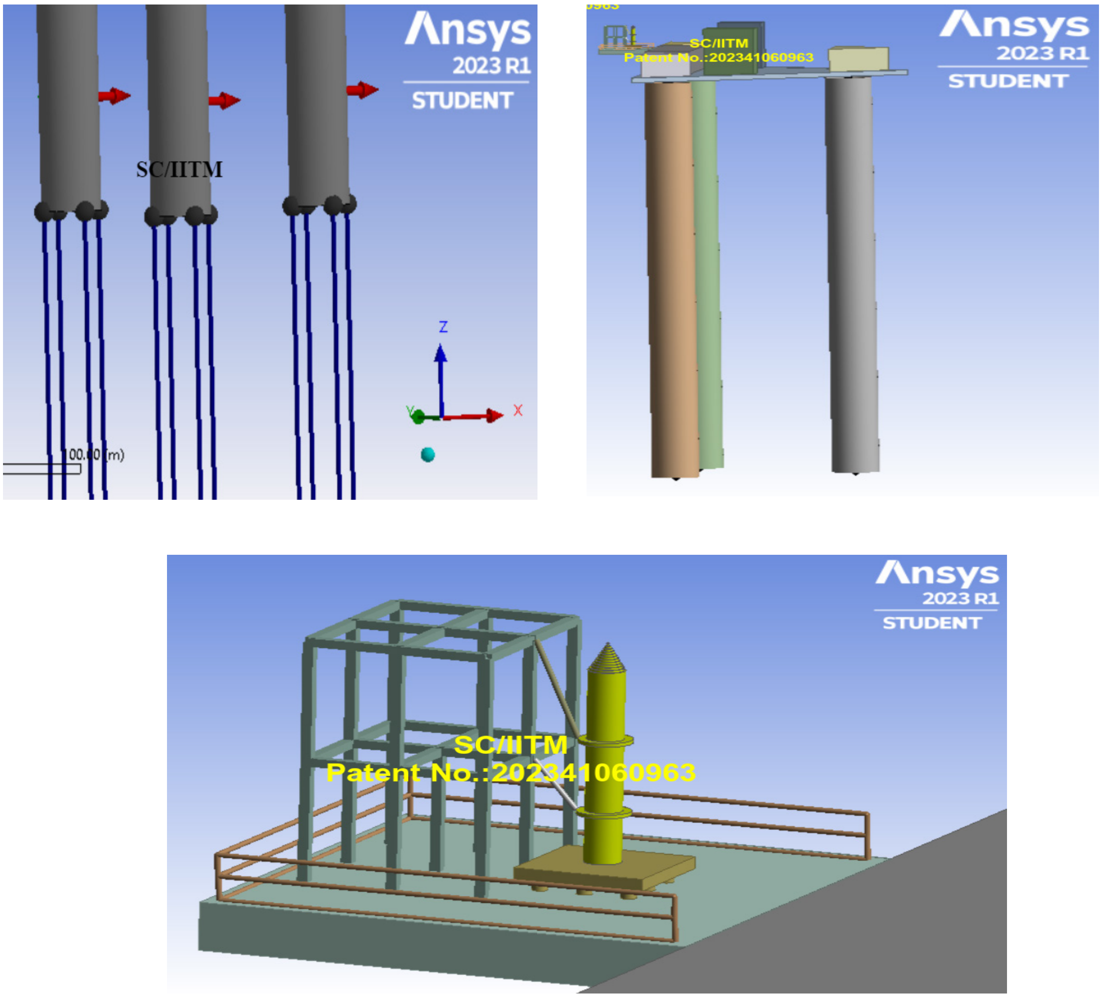

Figure 3 Numerical model of rocket launching Triceratops$^{\text{patented}}$ platform (Patent No.: 202341060963).

Table 2 Dynamic characteristics of deck with proposed missile launcher.

Description	Present study	Reference study (Chandrasekaran & Rao, 2019)
	Time Period (s)	**Time Period (s)**
Surge	156.8	133.0
Heave	3.0	3.2
Pitch	3.0	3.1

3.2 Response analysis

The time response analysis examines four scenarios of tether failure: no tether failure, single tether failure, and both sequential and simultaneous tether failure conditions. In the case of single tether failure, one tether connected to leg 1 experiences failure. The sequential failure scenario involves two tethers on leg 1 failing at different times. Conversely, in the simultaneous failure scenario, both tethers on leg 1 fail at the same time. Tethers on legs 2 and 3 remain unaffected in all scenarios.

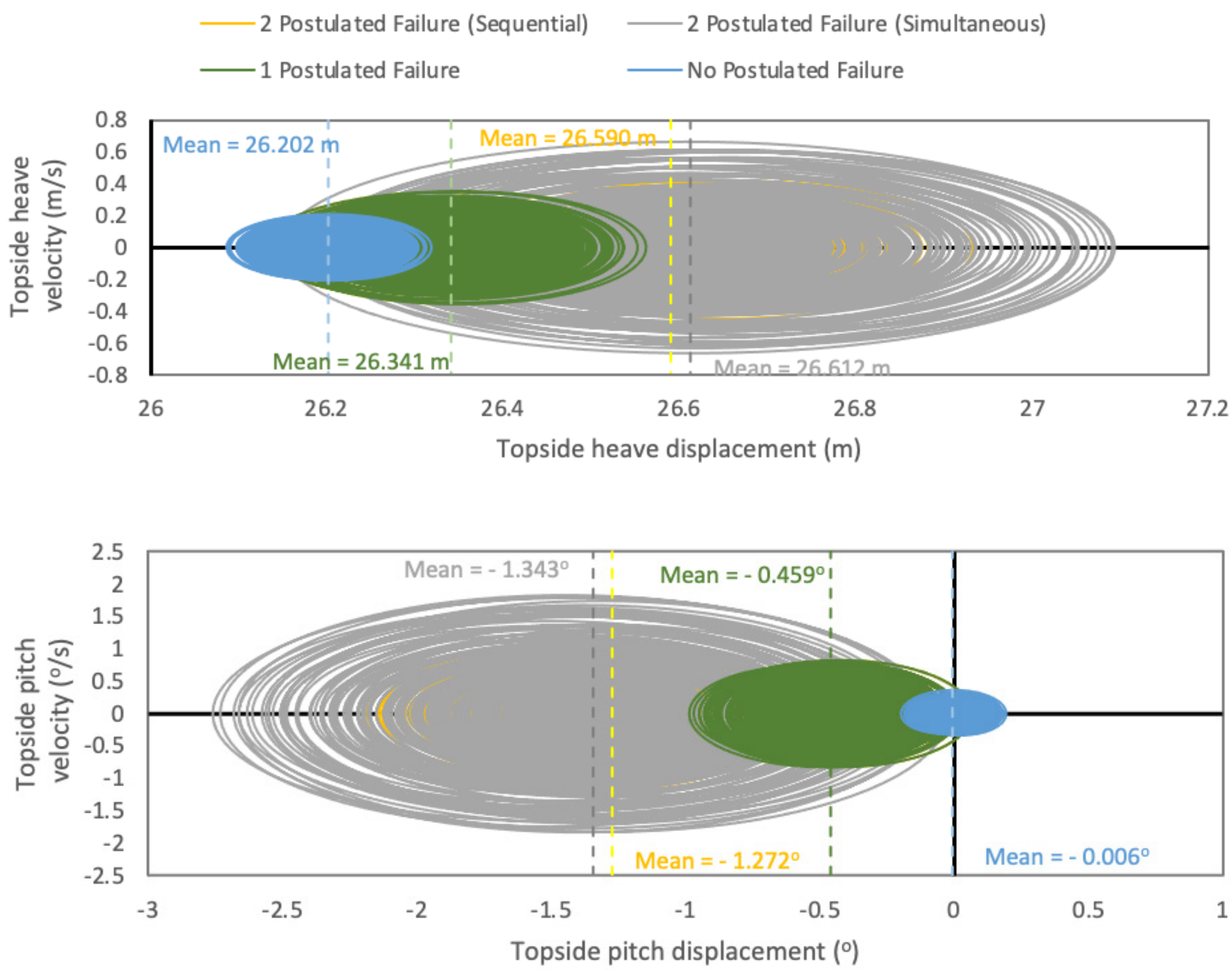

Figure 4 Phase plots of topside during rocket launch for various tether postulated failure conditions.

The phase plot analysis is conducted for the topside and buoyant legs by plotting the instantaneous velocity and corresponding displacements. Notably, the topside's center of gravity is 26.2 m above the mean sea level. When tethers are removed, a shift in the mean position is registered. Additionally, the width and height of the phase plots change, indicating that the responses in the altered conditions span a broader range compared to the intact state, which is concentrated in a small circle. Furthermore, the plots are symmetric about the vertical axis, demonstrating the structure's recentering capability. This symmetry is attributed to the high tension in the tethers, which helps restore the structure to its original position. Finally, the smooth elliptical shape of the phase plots reflects the platform's stability. The topside in heave response is stable even when two tethers fail simultaneously, despite a mean position change of 0.410 m (**Figure 4**). Additionally, the average value for sequential tether failure is slightly lower than that for simultaneous failure.

Similarly, in the case of topside pitch, phase plots demonstrate the highest mean variation when two tethers fail simultaneously, whereas the lowest variation is observed in the intact condition. The elliptical shape of the phase plot confirms the structural stability in the pitch degrees of freedom.

Leg 1 exhibits a similar response in the heave degree of freedom (**Figure 5**). However, in terms of pitch motion, the behavior has lost its smooth elliptical shape, suggesting a trend toward instability, although this instability has not yet occurred. Since the failed tethers were initially connected to leg 1, their removal resulted in a shift in the mean heave position, attributed to the changes in tether tension in the remaining tethers on that leg. In contrast, leg 2, which maintained intact tethers throughout the analysis, shows no significant changes in mean heave or pitch (**Figure 6**).

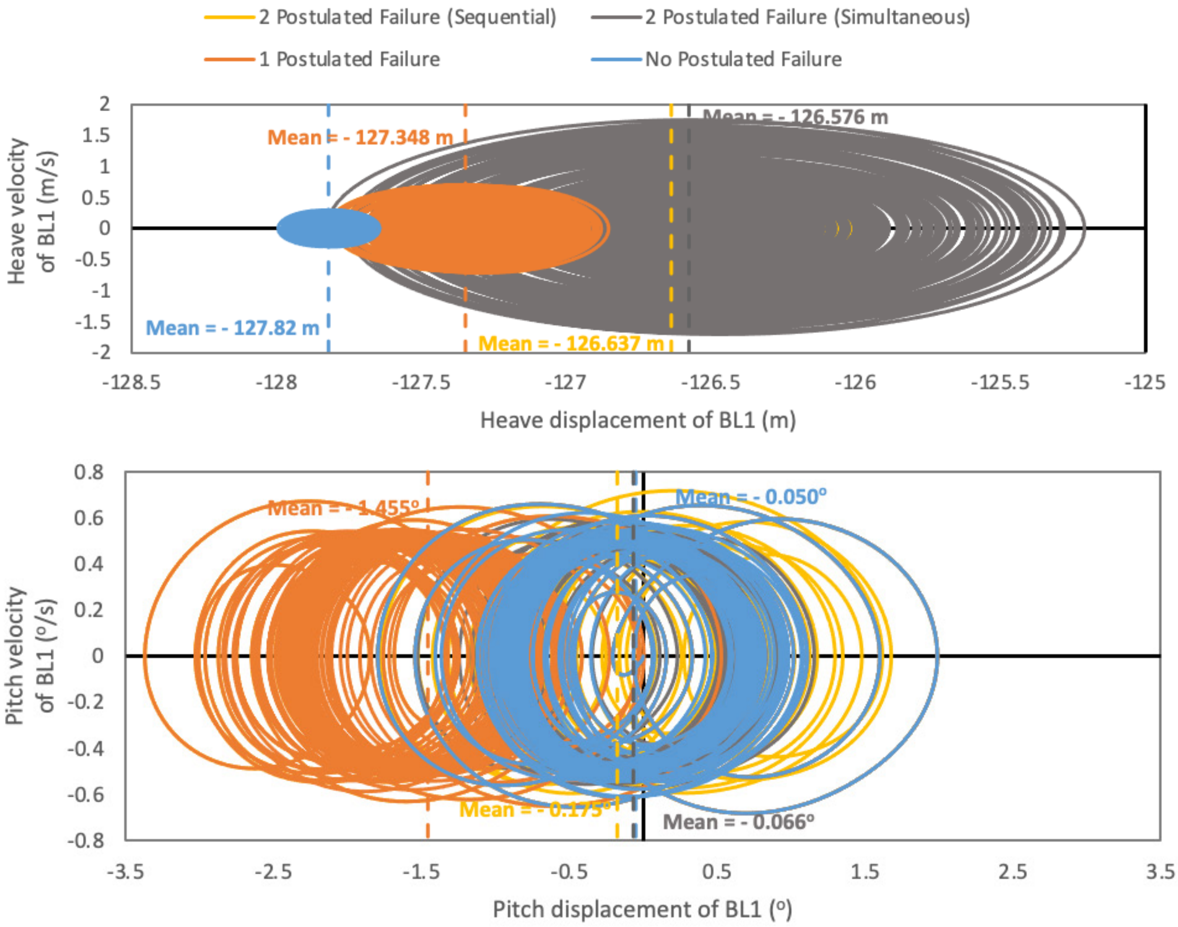

Figure 5 Phase plots of buoyant leg 1 (BL1) during rocket launch for various tether postulated failure conditions.

Interestingly, the pitch motion at the topside mirrors the heave motion of leg 1 rather than that of the legs themselves. Additionally, the topside pitch remains highly stable even under severe tether failure conditions, indicating that the structure is effectively insulated from the effects of tether instability, meaning the topside does not experience the instabilities caused by tether removal. This behavior can be attributed to the three-axis pivot joint, which isolates the structure from underwater phenomena. Despite this isolation, topside pitch motion is still present, though the legs' pitch motion does not influence it due to this isolation. Instead, the observed pitch motion at the topside is a result of the differential heave among the legs.

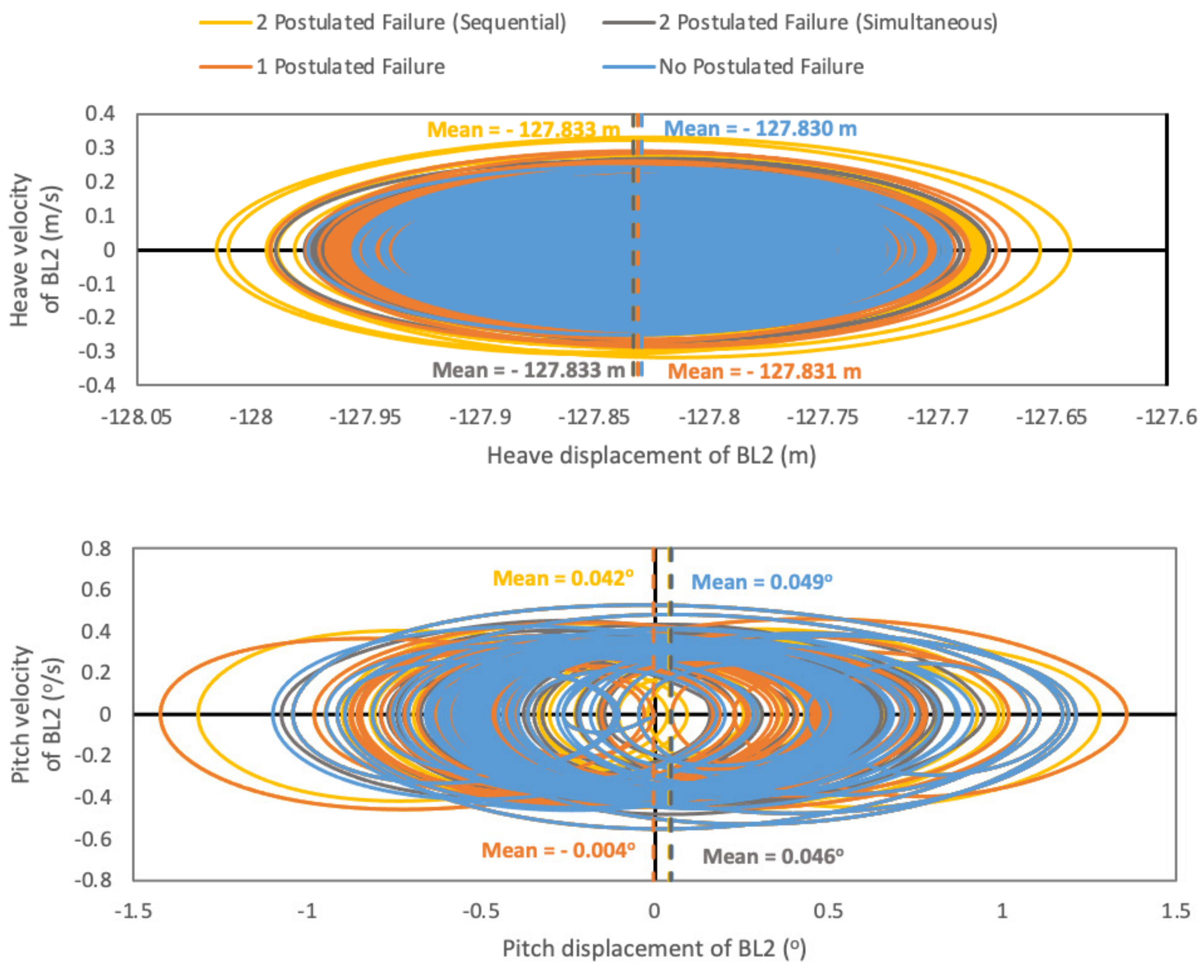

Figure 6 Phase plots of buoyant leg 2 (BL2) during rocket launch for various tether postulated failure conditions.

Specifically, while leg 2, which retains its tethers, does not experience a shift in its mean position, leg 1 does, creating a pitching effect on the topside due to the difference in heave between the legs.

3.3 Tether tension and stability analysis

Figure 7 displays the tension in different tethers under various failure scenarios during a space launch. Tether 2 is linked to buoyant leg 1, which experiences tendon failure, while tether 6 is attached to buoyant leg 2, whose tendons remain intact.

Table 3 Tether 2 and 6 tension variation parameters for various postulated failures.

Description	No postulated failure		Single postulated failure		Simultaneous postulated failure		Sequential postulated failure	
	T2	T6	T2	T6	T2	T6	T2	T6
Avg. tether tension, P (MN)	21.5	21.4	29.2	21.4	41.2	21.3	40.2	21.3
Amplitude of tether tension variation, S (MN)	2.80	2.30	8.85	2.58	21.5	2.47	19.9	3.01
Natural frequency of tether, $\bar{\omega}$ (rad/s)	0.47	0.47	0.55	0.47	0.65	0.47	0.65	0.47

For tether 2, the average tension is lowest when all tethers are operational, but it spikes when tethers 1 and 3 fail at the same time. Thus, the most critical situation for tether 2 occurs with the concurrent failure of tethers 1 and 3. Additionally, the impact of tether failures on tethers 2 and 6 varies significantly due to their connections to different buoyant legs. While tether 2 experiences fluctuations in tension, tether 6 remains unaffected by these changes. This suggests that failures in tethers significantly alter the tension and response of the buoyant legs associated with the failed tethers. When tethers fail, the remaining ones on the same leg experience increased tension as the load, once distributed among four tethers, is now shared by only two or three, depending on how many have failed. In contrast, the tethers on the other legs are largely unaffected, maintaining a relatively stable mean tension.

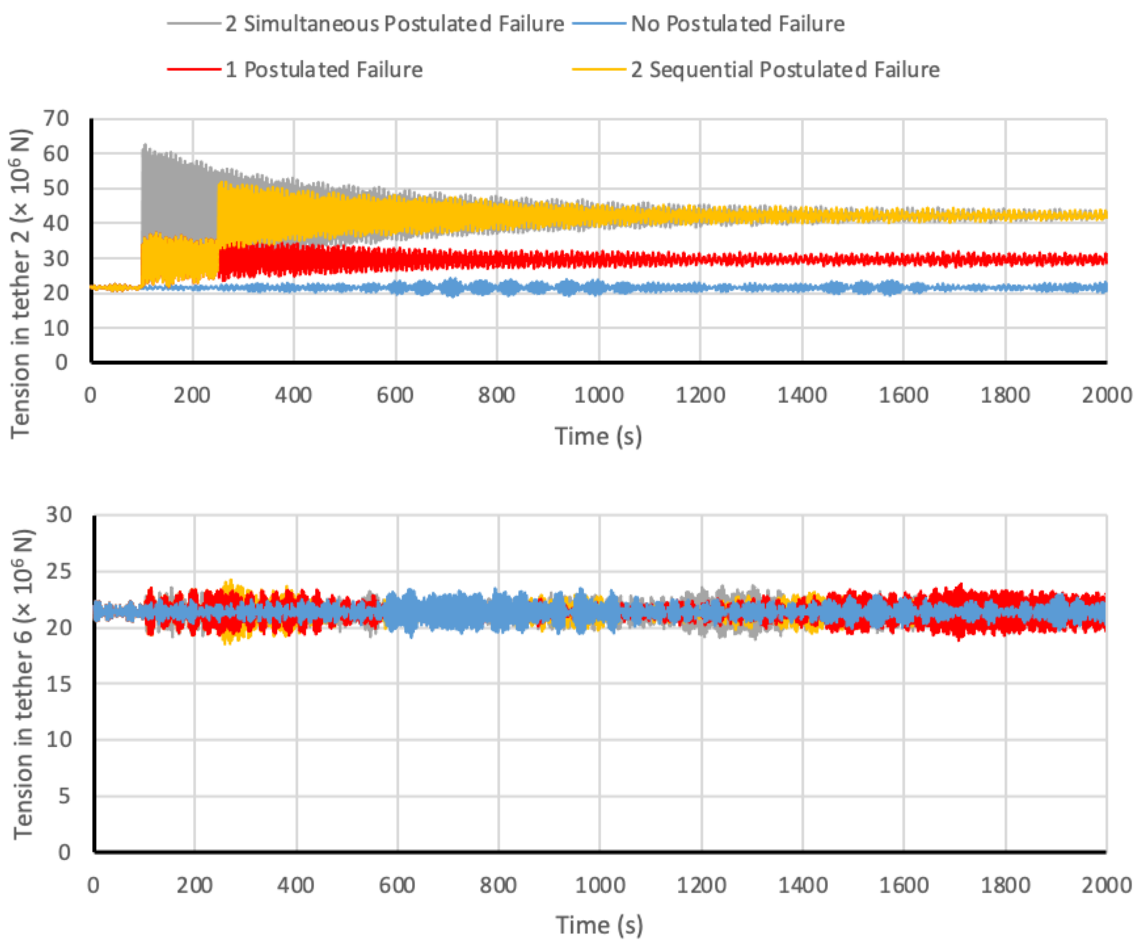

Figure 7 Tether tension during rocket launch for various tether postulated failure conditions.

Three scenarios of potential failures occurring after the rocket launch are examined to assess the tension variations in tethers 2 and 6. The parameters related to dynamic tether tension variations are provided in **Table 3**. The tether has a mass of 188.4 kg/m and a length of 2,246 m, with a wave frequency of 0.628 rad/s. These factors are integrated into the stability parameters from Eq. (2) to evaluate the tethers' stability. This analysis yields the stability parameters, as shown in **Table 4**. The corresponding data points are then represented in Mathieu's stability chart (**Figure 8**). The stable region is indicated by the area enclosed by the red and blue curves along with the horizontal axis.

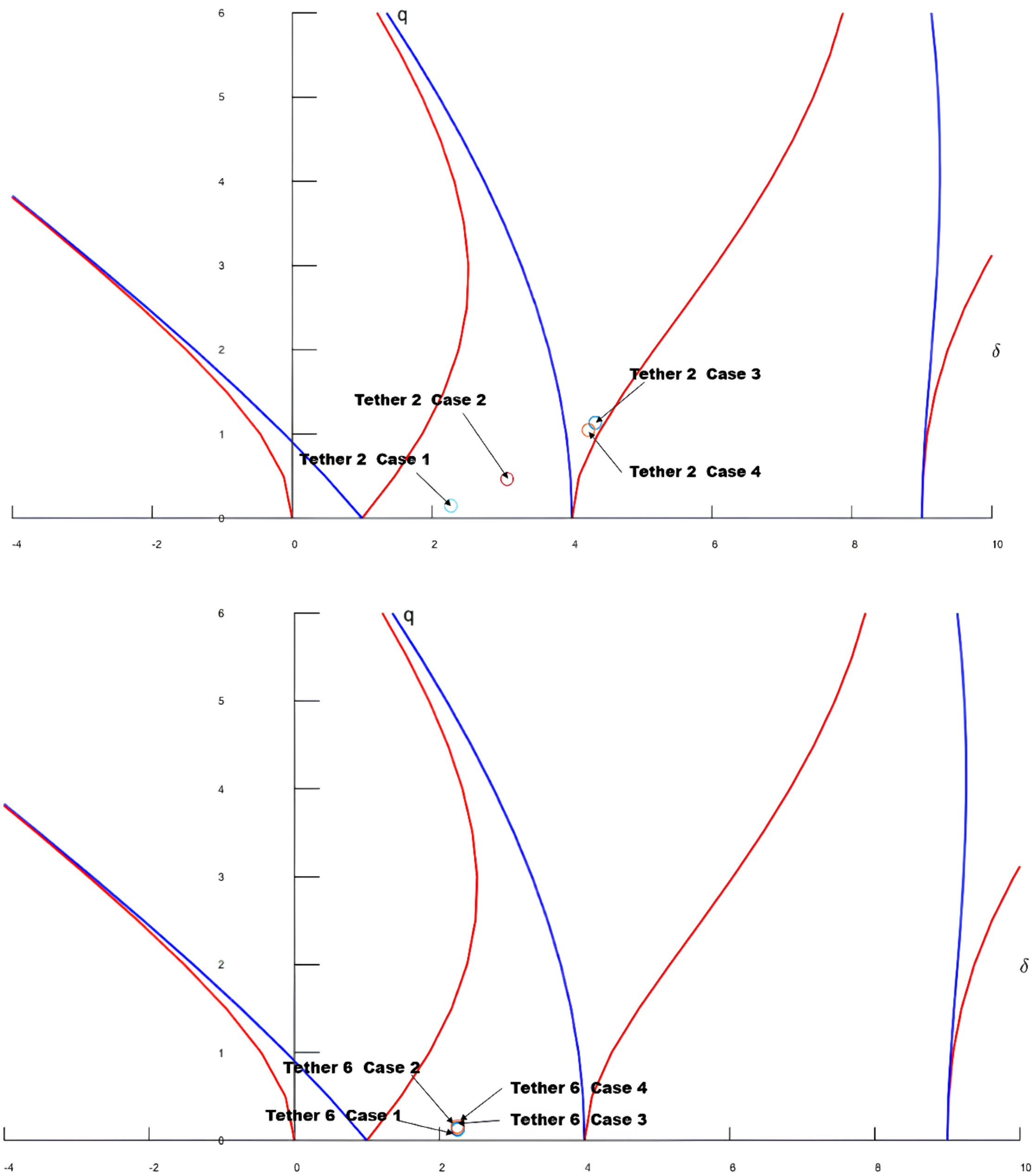

Figure 8 Stability chart for Triceratops tether 2 and 6 under postulated failure cases post-rocket launch.

According to Mathieu's stability chart, tether 6 remains stable across all proposed tether removal scenarios. In contrast, tether 2 shows stability only when all tethers are intact, or in cases of a single tether failure. The scenarios involving simultaneous or sequential failures are classified as unstable for tether 2, primarily because of the substantial increase in tension and elevated mean tension values observed (**Figure 7**). Additionally, the shock experienced by leg 1 during the failure of two tethers further exacerbates the instability in both simultaneous and sequential failure scenarios.

Table 4 Mathieu parameters for tether 2 and 6 for different postulated failure conditions post rocket launch.

Description	**Mathieu parameters**				**Stability condition**	
	δ		***q***			
	T2	**T6**	**T2**	**T6**	**T2**	**T6**
Case 1 (No postulated failure)	2.27	2.25	0.15	0.12	stable	stable
Case 2 (Single postulated failure)	3.07	2.25	0.47	0.13	stable	stable
Case 3 (Simultaneous postulated failure)	4.33	2.25	1.13	0.14	unstable	stable
Case 4 (Sequential postulated failure)	4.23	2.25	1.05	0.16	unstable	stable

4. Conclusions

This research performed a stability and tether analysis of the Triceratops under various anticipated tether removal scenarios following a rocket launch.

1) The free-decay tests confirmed that the platform's natural period for surge (~150 s) indicates flexible behavior, while the heave and pitch responses (~3 s) show high rigidity due to tether constraints.

2) The platform's response to different tether failure scenarios was analyzed, including no tether failure, single tether failure, and both sequential and simultaneous tether failure. The phase plot analysis revealed that the topside's stability is maintained even when two tethers fail simultaneously, with a change in the mean position, but no significant loss of stability. The symmetrical, elliptical shape of the phase plots in both heave and pitch confirms the platform's ability to recenter, and demonstrates its overall stability under failure conditions.

3) The behavior of leg 1, particularly in terms of heave, was found to be more sensitive to tether failure, exhibiting a shift in mean position. However, the topside's pitch motion remains stable even under severe tether failure conditions. This stability is attributed to the isolation provided by the three-axis pivot joint, which prevents the tether instability from being transferred to the topside. The differential heave between legs 1 and 2 induces a pitch motion on the topside, but this is not caused by instability in the legs themselves. Furthermore, the chaotic leg 1 pitch motion is not transferred to the topside, which showcases a smooth elliptical phase diagram.

4) The tether tension analysis revealed that tether 2, associated with leg 1, experiences the highest fluctuations in tension during simultaneous tether failures, while tether 6, associated with leg 2, remains largely unaffected. This finding underscores the significant impact of tether failure on the tension distribution, especially on the affected buoyant leg. The stability of the tethers was further assessed using Mathieu's stability chart. Tether 6 remained stable across all failure scenarios, while tether 2 showed stability only in the intact or single failure conditions. Sequential and simultaneous tether failures were classified as unstable for tether 2 due to the increased tension and shock experienced by the system.

Although the study demonstrates stable behavior of the topside under certain tether failure scenarios, the platform's overall safety in the event of multiple tether failures (e.g., two or more tethers) depends on various factors, including the magnitude and direction of the applied loads, the configuration of the remaining tethers, and the overall design of the platform. While the analysis indicates that the platform remains stable with limited tether failures, the failure of multiple tethers, particularly those connected to the most affected buoyant legs, could compromise the platform's stability. This study primarily focused on the stability of the platform under a specific set of conditions, and further analysis is needed to assess the safety of the platform under more severe failure scenarios. Future research should explore these conditions in greater detail to fully evaluate the potential risks and establish safety margins for multi-tether failures. This will help provide a more comprehensive understanding of the platform's performance under extreme conditions.

Moreover, this study primarily focused on the hydrodynamic behavior and stability analysis of the offshore platform under typical sea conditions, rocket load, and tether failure scenarios. However, a detailed investigation into the platform’s responses under varying operational and environmental load combinations, such as combined wave, wind, current, and rocket thrust loads, has not been performed. Future studies could address these load conditions to provide a more comprehensive understanding of the platform's dynamic behavior.

Furthermore, the hydro-elastic behavior of the structure was not considered, with the buoyant legs treated as rigid, and neglecting member and local element bending effects caused by waves and currents. The topside was assumed to act as a single rigid body throughout the rocket launch, which may oversimplify its actual dynamic response. Additionally, the impact of heat generated during the rocket launch on the platform's mechanical properties was excluded, disregarding potential degradation in strength, stiffness, or elastic modulus due to thermal exposure. These limitations highlight areas for further investigation, and future research should focus on incorporating hydro-elastic effects, flexible topside behavior, thermal impacts during launches, and more comprehensive dynamic modeling to improve accuracy.

Acknowledgments

This research received a specific grant from the Prime Minister Research Fund to the second author (PMRF), Govt. of India.

References

Allievi, A., & Soudack, A. (1990). Ship stability via the Mathieu equation. *International Journal of Control*, *51*(1), 139-167. https://doi.org/10.1080/00207179008934054

Anusree, A., & Sanil Kumar, V. (2023). Variations in short-term statistics of waves observed in the coastal waters of the eastern Arabian Sea. *Ocean Engineering, 281*, 114824. https://doi.org/10.1016/j.oceaneng.2023.114824

Ashish, P. U., Chandrasekaran, S., & Giorgio, S. (2024). Parametric study on the deep ocean space-rocket launching triceratops. *Ocean Engineering*, *295*, 116946. https://doi.org/10.1016/j.oceaneng.2024.116946

Chandrasekaran, S., & Chinu, P. (2023). Dynamic analysis of offshore triceratops supporting wind turbine: Preliminary studies. *Maritime Technology and Research*, *6*(1), 265564. https://doi.org/10.33175/mtr.2024.265564

Chandrasekaran, S., & Rao, M. (2019). Numerical analysis on Triceratops restraining system: failure conditions of tethers. *International Journal of Environmental and Ecological Engineering, 13*(9), 588-592. https://doi.org/10.5281/zenodo.3461996

Chandrasekaran, S., & Kiran, P. A. (2018). Mathieu stability of offshore triceratops under postulated failure. *Ships and Offshore Structures, 13*(2), 143-148. https://doi.org/10.1080/17445302.2017.1335578

Chandrasekaran, S. (2017). *Dynamic analysis and design of ocean structures* (2nd Ed.). Singapore: Springer. https://doi.org/10.1007/978-981-10-6089-2

Chandrasekaran, S., & Mayanak, S. (2016). Dynamic analyses of stiffened triceratops under regular waves: experimental investigations. *Ships and Offshore Structures, 12*(5), 697-705. https://doi.org/10.1080/17445302.2016.1200957

Chandrasekaran, S., Madhuri, S., & Jain, A. K. (2013). Aerodynamic response of offshore Triceratops. *Ship and Offshore Structures, 8*(2), 123-140. https://doi.org/10.1080/17445302.2012.691271

Haitao, W., Zhiyang, Z., Weixing, L., Lin, C. (2023). Effects of tendon breakage on the dynamic behavior of a TLP. *Ships and Offshore Structures, 19*(7), 882-891. https://doi.org/10.1080/17445302.2023.2218319

Kolukula, S. S. (2012). *Stability chart*. MATLAB Central File Exchange, Version 1.1.0.0, MathWorks. Retrieved from https://www.mathworks.com/matlabcentral/fileexchange/35355-stability-chart

Koo, B. J., Kim, M. H., & Randall, R. E. (2004). Mathieu instability of a spar platform with mooring and risers. *Ocean Engineering, 31*(17-18), 2175-2208. http://doi.org/10.1016/j.oceaneng.2004.04.005

Mishra, D. (2017). *Fundamentals of rocket propulsion* (2nd eds.). Boca Raton: CRC Press. https://doi.org/10.1201/9781315175997

Newmark, N. M. (1959). A method of computation for structural dynamics. *Journal of Engineering Mechanics, ASCE, 85*(3), 67-94. https://doi.org/10.1061/JMCEA3.0000098

Patel, M. H., & Park, H. I. (1991). Dynamics of tension leg platform tethers at low tension, Part I - Mathieu stability at large parameters. *Marine Structures, 4*(3), 257-273. https://doi.org/10.1016/0951-8339(91)90004-U

Sabique, L., Annapurnaiah, K., Balakrishnan Nair, T. M., & Srinivas, K. (2012). Contribution of Southern Indian Ocean swells on the wave heights in the Northern Indian Ocean-A modeling study. *Ocean Engineering, 43*, 113-120. https://doi.org/10.1016/j.oceaneng.2011.12.024

Suja, T. P., & Chandrasekaran, S. (2025). Response control of TLP with single TMD under wind, wave, and current. *Maritime Technology Research, 7*(1). https://doi.org/10.33175/mtr.2025.272515

Zhengyu, S., Zhifeng, X., Limin, Q., Dalin, X., & Jinglin, L. (2021). Prospects of sea launches for Chinese cryogenic liquid-fueled medium-lift launch vehicles. *Chinese Journal of Aeronautics, 34*(1), 424-437. http://doi.org/10.1016/j.cja.2020.06.018